The Egyptian Journal of Remote Sensing and Space Sciences 28 (2025) 587–596

Contents lists available at ScienceDirect

The Egyptian Journal of Remote Sensing and Space Sciences

journal homepage: www.sciencedirect.com

Research Paper

A multi-criteria GIS model for geohazard assessment in the Charvak reservoir area, Uzbekistan

Dilbarkhon Fazilova [a,b,e,*], Khasan Magdiev [a,c], Mirshodjon Makhmudov [a], Alisher Fazilov [d]

[a] Ulugh Beg Astronomical Institute of Uzbekistan Academy of Sciences, 33 Astronomy Street, 100052 Tashkent, Republic of Uzbekistan
[b] Tashkent State Technical University Named After Islam Karimov, 2 University Street, 100095 Tashkent, Republic of Uzbekistan
[c] Ministry of Economy and Financial of the Republic Uzbekistan, Istiqlol street 29, 100017 Tashkent, Republic of Uzbekistan
[d] Tashkent University of Architecture and Civil Engineering, 9A Yunusabad District, Yangishahar Street, 100194 Tashkent, Republic of Uzbekistan
[e] National University of Uzbekistan named after Mirzo Ulugbek, University street 4, 100174 Tashkent, Republic of Uzbekistan

ARTICLE INFO

Keywords:
Slope instability
Landsat
SRTM
AHP
NDWI
Active faults

ABSTRACT

Mountainous reservoir regions are particularly susceptible to geohazards due to steep topography, fractured lithologies, active faults, and seasonal hydrological fluctuations. The Charvak basin in northeastern Uzbekistan, designated as a Free Tourist Recreation Zone, is increasingly affected by expanding infrastructure and tourism, which increases exposure to natural hazards. This study presents the first integrated geohazard susceptibility map of the Charvak basin using remote sensing and multi-criteria GIS analysis. A GIS-based model was developed to evaluate slope-related hazards—landslides, debris flows, and rockfalls—based on six indicators: slope gradient, lithological strength, lineament density, Normalized Difference Water Index (NDWI), distance to active faults, and distance to the reservoir shoreline. The indicators were weighted using the Analytic Hierarchy Process (AHP), with slope gradient (0.28) and lineament density (0.24) identified as dominant factors. The resulting composite index was validated through comparison with landslide and debris flow inventories as well as seismicity data. The susceptibility map indicates that ~19 % of the basin falls into high and very high hazard classes, while ~48 % is classified as low to very low. High-susceptibility zones overlap substantially with infrastructure, including 21 % of villages and tourism facilities and 27 % of the road network. These findings provide a spatial basis for risk-informed land-use regulation, infrastructure planning, and disaster management in the Charvak region. More broadly, the study demonstrates the effectiveness of combining remote sensing and multi-criteria GIS methods for geohazard assessment in other mountainous and data-limited environments.

1. Introduction

Geohazard assessment in mountainous and tectonically active regions is a critical research task, as these environments are among the most vulnerable to natural hazards that threaten human settlements, infrastructure, and sustainable development (Kumari et al., 2022; Ramachandra et al., 2016; Ye et al., 2024). Effective evaluation requires the integration of geomorphological, structural, hydrological, and anthropogenic factors within a spatial analysis framework.

In this study, the focus is on slope-related processes—landslides, debris flows, and rockfalls—which represent the most frequent and damaging hazards in steep mountain environments (Gill and Malamud, 2014; Pospíšil et al., 2025; Reichenbach et al., 2018). Identifying hazard-prone zones is essential for safe territorial development, as demonstrated in previous multi-hazard assessment studies (Bachri et al., 2024; Bathrellos et al., 2017; Karpouza et al., 2023; Leonardi et al., 2022; Skilodimou et al., 2019).

The Charvak Reservoir basin in northeastern Uzbekistan represents such a high-risk environment. Situated in the western Tien Shan, it combines steep terrain (Fazilova et al., 2021; Sharipov et al., 2020), active fault zones (Bellendir and Aleksandrov, 2023; Fazilova et al., 2025; Khamidov et al., 2021; Makhmudov and Fazilova, 2023), complex lithology (Umurzakov and Muminov, 2017), and pronounced seasonal hydrological fluctuations (Khamidov et al., 2023; Plotnikova et al., 1992; Sichugova and Fazilova, 2020). In 2017, the region was designated as a Free Tourist Recreation Zone,[1] which now hosts more than

* Corresponding author at: Ulugh Beg Astronomical Institute of Uzbekistan Academy of Sciences, 33 Astronomy Street, 100052 Tashkent, Republic of Uzbekistan.
E-mail address: dil_faz@yahoo.com (D. Fazilova).

[1] On the establishment of the free tourist zone "Charvak" [Decree of the President of the Republic of Uzbekistan. No. PQ-3441, December 5, 2017]. Retrieved from https://lex.uz/docs/3441087.

https://doi.org/10.1016/j.ejrs.2025.09.003
Received 9 July 2025; Received in revised form 21 August 2025; Accepted 7 September 2025
Available online 11 September 2025

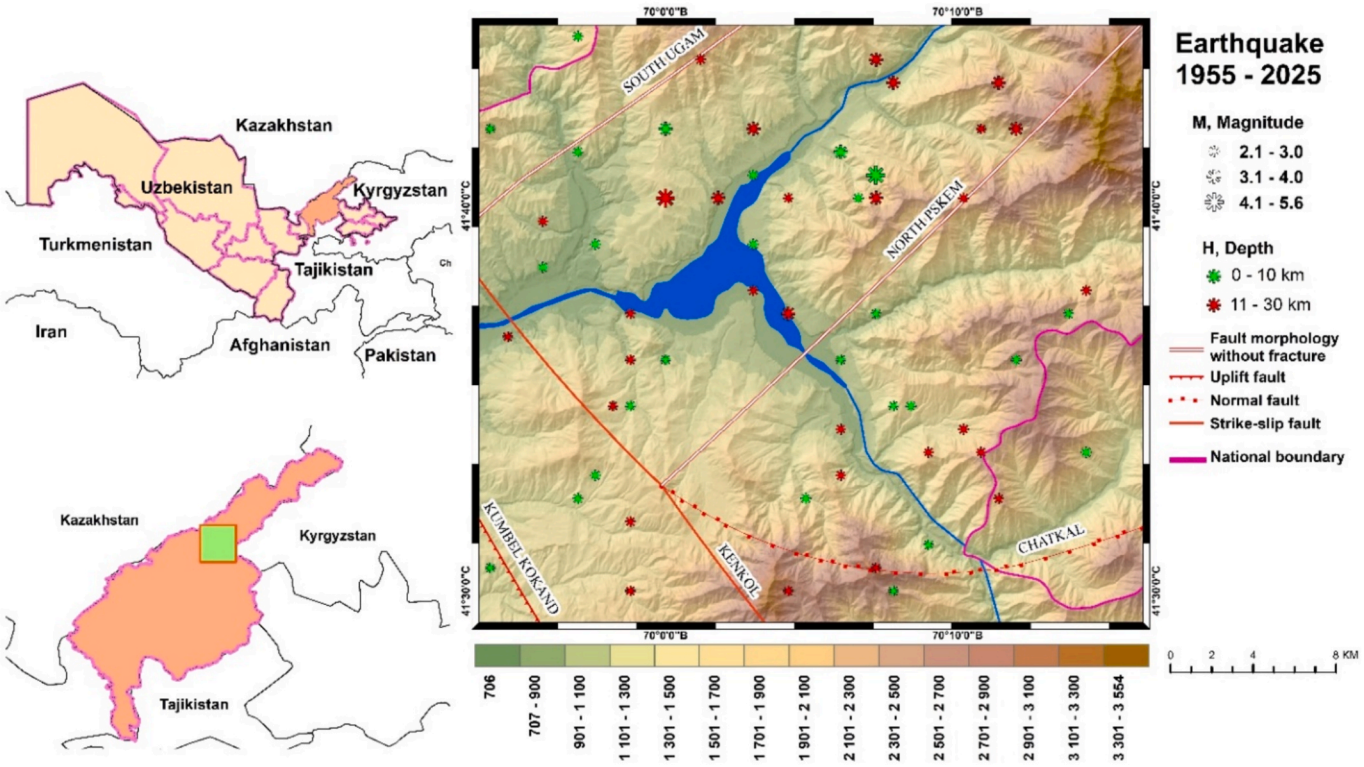

Fig. 1. Geographical location of the Charvak Reservoir in Central Asia (top-left) and within the Tashkent Region (bottom-left); regional tectonic framework (Tsay, 2019) and distribution of earthquakes from 1955 to 2025 (right)[3]. [3]Republican Center for Seismic Prognostic Monitoring (RCSPM) database. http://www.smrm.uz/?lang=ru, (accessed 07 January 2025).

180 tourist facilities, 40 villages, about 10,000 households, and 240 km of roads (Juliev et al., 2019). The rapid expansion of infrastructure along steep reservoir-facing slopes has heightened exposure to hazards and created an urgent demand for risk-informed territorial planning. At the same time, land cover dynamics indicate pressure on sensitive terrain: between 1989 and 2017 forest cover increased slightly, built-up areas grew from 1.7 % to 2.3 %, while snow and bare land declined. These changes reflect combined climatic and anthropogenic influences (Alikhanov et al., 2020; Juliev et al., 2019). Despite its ecological and socioeconomic importance, no integrated susceptibility maps exist for the Charvak basin. Previous studies considered individual components of instability, but did not provide a spatially explicit multi-criteria assessment (Juliev et al., 2019; Khamidov et al., 2023; Petrov et al. 2017). Limited ground monitoring further underlines the need for satellite-based approaches that provide consistent and wide coverage.

Remote sensing and GIS offer such a framework. Methods commonly applied include statistical models, machine learning, and physically based simulations. While effective, their use in data-scarce mountain regions is constrained by data gaps and interpretability issues (Chen et al., 2015; Cheng et al., 2022; Cui et al., 2024; Dong et al., 2011; Zandi and Pari Far, 2025). The Analytic Hierarchy Process (AHP) (Saaty, 1990) provides transparent prioritization of variables and has been successfully applied in landslide mapping (Bera et al., 2019; Kadapa, 2024), seismic zonation (Fentahun et al., 2021; Hu et al., 2018; Jena and Pradhan, 2020; Skilodimou et al., 2019), and flood hazard assessments (Al-Taani et al., 2023; Elkhrachy, 2015; Skilodimou et al., 2019). Its flexibility under data-limited conditions makes AHP particularly suitable for the Charvak basin, as also demonstrated in broader hydro-geomorphological and environmental hazard studies (Mokhtari et al., 2017; Zzaman et al., 2021).

The aim of this study is to develop a GIS-based multi-criteria model for geohazard assessment in the Charvak Reservoir region using AHP. Specific objectives are: (i) to select and preprocess six indicators relevant to slope instability (slope gradient, lithological strength, lineament density, NDWI, distance to active faults, and distance to the reservoir shoreline); (ii) to normalize and weight these indicators; (iii) to integrate them into a composite hazard index; and (iv) to validate the results against landslide inventories, seismic records, and land cover data.

2. Materials and method

2.1. Study area

The study area encompasses the Charvak Reservoir and its surroundings in northeastern Uzbekistan, within the western Tien Shan, a tectonically active zone formed by the convergence of the Eurasian and Indian lithospheric plates (Wu et al., 2023). The reservoir, formed at the confluence of the Chatkal, Pskem, and Koksu rivers, covers 37.3 km^2 with a maximum depth of 150 m.[2] Elevations range from 710 to over 3550 m, and the landscape is dominated by steep slopes and incised valleys (Fig. 1).

The basin is intersected by several active fault systems—notably the Kumbel–Ugam, Chatkal, and Pskem—which demonstrate late Cenozoic tectonic activity, including displaced terraces and historical seismicity (Khamidov et al., 2021). Recent GNSS and morphotectonic studies further confirm their ongoing activity, with horizontal velocities of 4–5 mm/yr and localized strain accumulation along the Kumbel–Ugam and North Pskem faults (Fazilova et al., 2025; Juliev et al., 2017; Khamidov et al., 2021; Umurzakov, 2012). Seismic records (1955–2025) indicate magnitudes up to 5.6 at shallow depths, clustered along fault zones and reservoir margins (Khamidov et al., 2021).

The reservoir's hydrology follows a distinct seasonal cycle: peak water levels in July from snowmelt, progressive drawdown from August

[2] https://www.fao.org 〉 water 〉 aquastat 〉 dams 〉 country 〉 UZB-dams_eng.

Table 1
Spatial indicators used in the geohazard model, with descriptions, data sources, and supporting references.

Criterion	Description	Data source	References
Slope Gradient	Quantifies terrain steepness; steeper slopes are more prone to gravitational instability and	SRTM DEM	Arabameri et al., 2018; Fentahun et al., 2021; Verma and Patel, 2021
Lithological Strength	Represents mechanical strength of surface materials; weak or fractured rocks are more susceptible to failure.	Geological map	Abella and Van Westen, 2007
NDWI	Spectral moisture index derived from Landsat (Green and NIR bands); used to assess seasonal saturation conditions and hydrological loading effects on slopes	Composite Landsat 5, 7, 8, and 9 Level-2 Surface Reflectance imagery (October scenes, 2000–2024), accessed via Google Earth Engine (GEE)	Arabameri et al., 2018; Das et al., 2022; Xu, 2006
Lineament Density	Measures spatial density of linear features; high values suggest structural discontinuities and stress concentration	Landsat 9 (SWIR)	Das et al., 2022; Fentahun et al., 2021;Romero-Andrade et al., 2023; Sichugova and Fazilova, 2021; Verma and Patel, 2021
Distance to Active Faults	Represents proximity to tectonic structures; closer distances may indicate increased deformation potential	Digitized fault lines	Fentahun et al., 2021; Lee and Evangelista, 2006
Distance to Reservoir Shoreline	Captures hydromechanical loading from reservoir fluctuations; proximity correlates with stress redistribution	Digitized reservoir	Arabameri et al., 2018; Gupta, 2022; Talwani, 1997

to October for irrigation and hydropower, and refillig beginning in March (Rakhmatullaev et al., 2013). The spatial extent was defined to include structurally and hydrologically connected terrain beyond the reservoir itself. This includes steep reservoir-facing slopes, and fault-controlled escarpments.

Overall, the study area integrates key geomorphic, lithological, and tectonic features necessary for evaluating compound slope-related geohazards in a high-relief, data-limited mountain environment.

2.2. Selection of risk indicators

To construct a geohazard model for the Charvak Reservoir region, six spatial indicators were selected for their relevance to slope instability. These reflect morphometric, structural, lithological, and hydrological factors commonly associated with geohazard development in mountainous and tectonically active settings (Table 1). The selection also accounted for data availability and resolution.

The inclusion of NDWI and lineament density compensates for the lack of high-resolution precipitation and hydrological records, offering indirect but spatially consistent indicators of moisture and structural activity. Together, these six indicators capture the dominant drivers of slope-related geohazards in the Charvak basin.

2.3. Data preprocessing and standardization

Geospatial data layers were obtained from publicly available sources and digitized thematic maps, resampled to 30-meter resolution and projected to WGS84/UTM Zone 42 N. Preprocessing included reprojection, cloud masking for satellite imagery, and spatial alignment (Fig. 2).

Slope was derived from the Shuttle Radar Topography Mission (SRTM) 1 Arc-Second Global DEM (30 m) using ArcGIS Spatial Analyst (Fig. 2a).

Normalized Difference Water Index (NDWI) was calculated from Landsat 5, 7, 8, and 9 surface reflectance data (2000–2024), filtered for scenes with < 20 % cloud cover over the Charvak region (Fig. 2b). To minimize noise from atmospheric variability and outliers, median composites were generated for each October, as this month corresponds to the reservoir's drawdown phase, when contrasts in slope saturation and surface moisture are most pronounced. Median compositing is a standard approach in multi-year remote sensing analysis, as it preserves stable surface signals while reducing artifacts from single scenes (Gao, 1996; Roy et al., 2010; White et al., 2014).

NDWI was computed using the formula $(\text{Green}-\text{NIR})/(\text{Green}+\text{NIR})$, based on bands SR_B2/SR_B4 (Landsat 5/7) and SR_B3/SR_B5 (Landsat 8/9) (Xu, 2006). Only pixels with NDWI > 0 were retained to emphasize saturated surfaces. Following established criteria (McFeeters, 1996; Xu, 2006) and adapted to the statistical distribution of values in the Charvak basin, NDWI values were divided into four intervals representing increasing soil moisture and water content (see Fig. 2b). Similar classification approaches have been applied in recent studies linking NDWI thresholds with slope instability and hydrological processes (Fang et al., 2021). This classification provides a consistent spatial indicator of surface moisture variability, which is critical for slope-related geohazard assessment in the Charvak basin.

Lineament density was derived from Landsat 9 SWIR-2 imagery (Band 7, 2.11–2.29 μm), obtained as Level-2 surface reflectance data from the USGS. Lineaments were extracted automatically using the open-source pyLefa tool (Shevyrev and Carranza, 2020), which applies edge detection and Hough transform algorithms. Default parameters optimized for SWIR-2 imagery were used. The short-wave infrared band was selected for its sensitivity to geological structures and reduced susceptibility to atmospheric effects (Moore, 1983) (Fig. 2c). It is important to note that not all extracted lineaments represent active tectonic faults. Validating them as active structures requires detailed field investigations and geophysical surveys. In this study, lineament density is therefore employed only as a proxy indicator of structural discontinuity and crustal weakness that may facilitate slope instability. This approach is consistent with previous applications in Central Asia (Fazilova et al., 2026).

Lithology was digitized from geological maps available in the USGS data catalog (scale of 1:180,000; Drummer, 1998) (Fig. 2d). For integration into the model, lithological units were reclassified into five ordinal stability classes based on their relative resistance to weathering and slope failure. Hard rock formations (e.g., intrusive and metamorphic rocks, limestone) were assigned higher stability values, while weaker units such as sandstone, clay, and Neogene–Quaternary deposits were ranked as less resistant. This classification was guided by the mechanical properties of the mapped formations and follows established approaches in landslide susceptibility mapping (Aleotti and Chowdhury, 1999; Dai et al., 2002).

Distance to active faults. Fault lines were digitized from tectonic and geological maps (Tsay, 2019) and converted into a raster layer using the Euclidean distance function in ArcGIS. Distances were inverted and normalized so that areas closer to faults received higher susceptibility values, reflecting their potential for increased deformation (Fig. 2e).

Distance to reservoir shoreline. The Charvak Reservoir boundary was digitized from 1:25,000 topographic maps, and Euclidean distances were calculated from each grid cell to the shoreline. Shorter distances were assigned higher susceptibility values to capture the effect of seasonal hydromechanical loading and pore-pressure changes associated with reservoir fluctuations (Gupta, 2022; Talwani, 1997) (Fig. 2f).

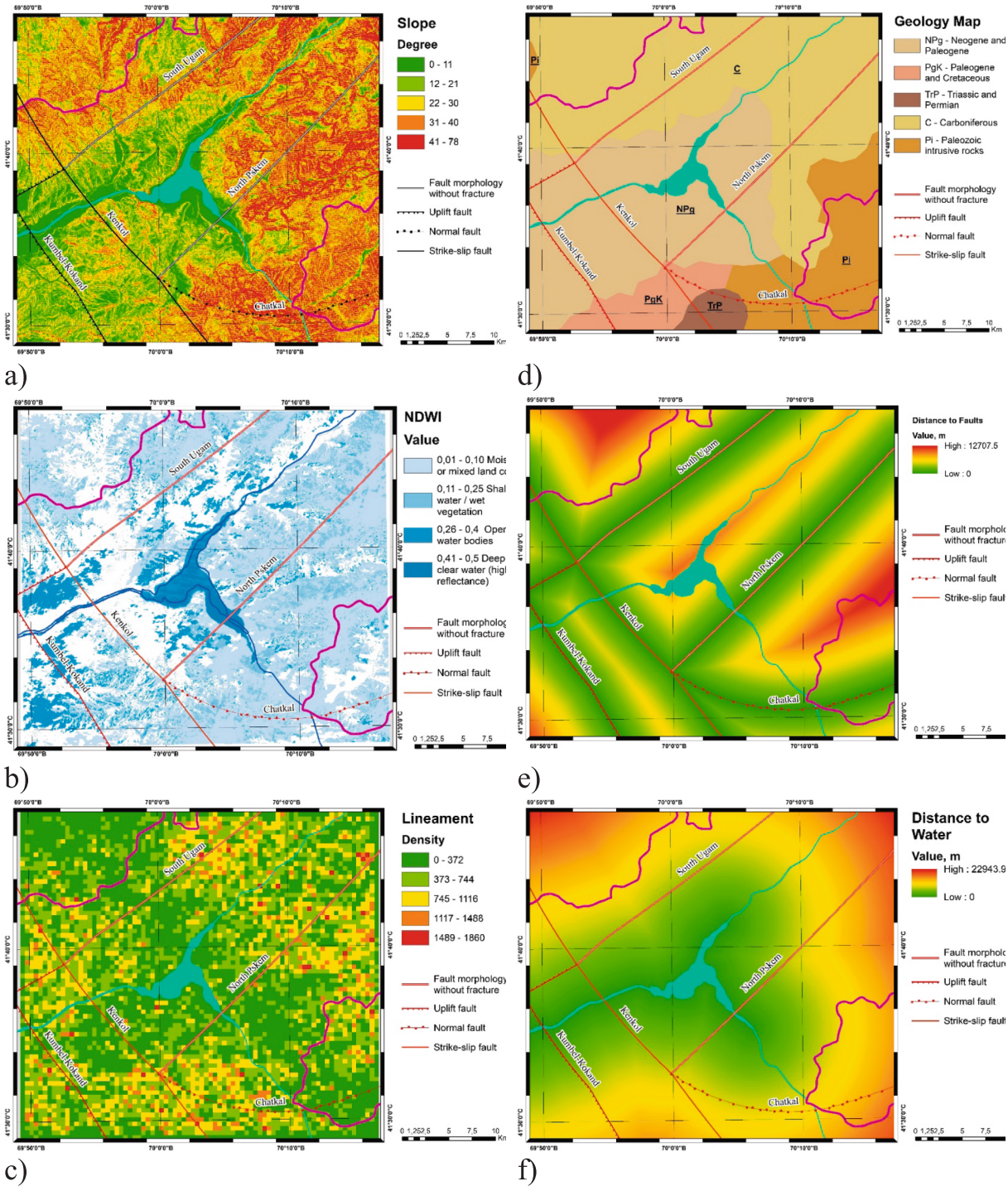

Fig. 2. Conditioning factors used in the multi-criteria hazard model: (a) Slope; (b) NDWI; (c) Lineament density; (d) Lithology; (e) Distance to faults; (f) Distance to reservoir.

Table 2
Summary statistics for geohazard indicators.

Indicator	Minimum	Maximum	Mean
Slope gradient (°)	0	71	23.5
Lithological strength (Rank)	1	5	3.1
NDWI (October)	0	0.96	0.11
Lineament density (count/km^2)	0	18.2	5.9
Distance to faults (km)	0	9.8	4.3
Distance to reservoir (km)	0	10.9	5.1

At the conclusion of the preprocessing stage, summary statistics were computed for each geohazard indicator prior to normalization. These values reflect the original range and distribution of the variables across the study area and are presented in Table 2.

2.4. Analytic hierarchy process (AHP) and weighting scheme

To integrate heterogeneous datasets, all input layers were normalized to a 0–1 scale. Continuous indicators (slope, NDWI, lineament density, distances) were rescaled using min–max normalization, while

Table 3
Pairwise comparison matrix of criteria and derived weights based on AHP (CR = 0.08).

Criteria	Slope	Lineament	NDWI	Lithology	Faults	Reservoir	Weight (%)
Slope	1	2	3	4	6	7	38.24
Lineament	1/2	1	2	3	4	5	25.17
NDWI	1/3	1/2	1	2	3	3	15.37
Lithology	1/4	1/3	1/2	1	2	2	9.54
Faults	1/6	1/4	1/3	1/2	1	2	6.36
Reservoir	1/7	1/5	1/3	1/2	1/2	1	5.32

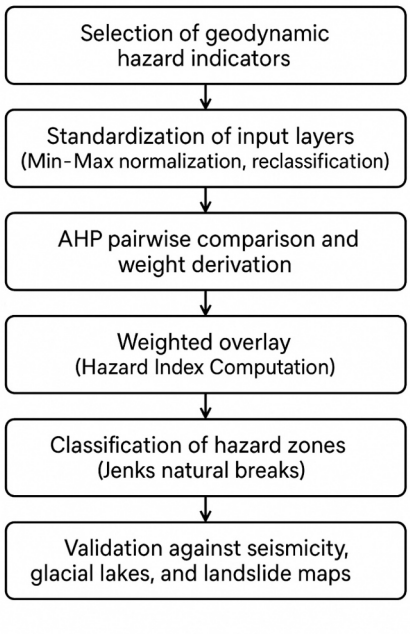

Fig. 3. Workflow diagram of the AHP-based geohazard assessment methodology.

lithological units were reclassified into ordinal stability classes (1–5) and normalized accordingly:

$$X_{norm} = \frac{X - X_{\min}}{X_{\max} - X_{\min}} \quad (1)$$

where X_{norm} is the normalized value, X the raw value, and $X_{\min}$ and $X_{\max}$ the minimum and maximum of the dataset.

For categorical variables (e.g., lithology), ordinal scores from 1 (stable) to 5 (least stable) were assigned based on mechanical properties and susceptibility to mass movement. The scores were then normalized as follows:

$$Score_{norm} = \frac{Score - 1}{4} \quad (2)$$

Relative weights of the six indicators were assigned using AHP. A pairwise comparison matrix was developed based on expert knowledge and previous geohazard studies (Arabameri et al., 2018; Bera et al., 2019; Jena and Pradhan, 2020). Importantly, the comparison also accounted for specific characteristics of the Charvak basin, including steep reservoir-facing slopes, lithological contrasts, proximity to fault systems, and seasonal reservoir-level fluctuations. The consistency of the comparison matrix was verified using the Consistency Ratio (CR = 0.08), which falls within the acceptable threshold (CR < 0.1). The final weighting scheme highlighted slope gradient and lineament density as dominant factors, while lithology, moisture conditions, and distance-based indicators played secondary roles (Table 3). While AHP provides a transparent and systematic approach, it is inherently sensitive to subjective expert judgment and assumes static relationships between factors. Moreover, accuracy is constrained by the resolution and completeness of input datasets. These limitations were partly mitigated by cross-validation among multiple experts, but they remain important considerations for interpretation.

2.5. Composite hazard index and mapping

The normalized and weighted indicators were integrated into a composite geohazard index using a weighted linear combination:

$$Risk\ Index = \sum_{i=1}^{n} (\omega_i \cdot X_{i,norm}) \quad (3)$$

where ω_i represents the AHP-derived weight of the ith factor, and $X_{i,\text{norm}}$ is the normalized value of factor *i*. This formulation ensures that areas with steep slopes, weak lithology, high lineament density, elevated surface moisture, and proximity to faults or the reservoir receive higher susceptibility scores.

The continuous hazard index was classified into five categories (very low, low, moderate, high, very high) using the Jenks natural breaks method, which minimizes intra-class variance and maximizes inter-class separation. The resulting map (Fig. 3) provides a spatial representation of slope-related geohazards in the Charvak basin (Jenks, 1967). The approach highlights zones where multiple risk factors converge, but should be interpreted as a relative susceptibility model rather than a deterministic prediction of future events. Field validation and integration of additional datasets (e.g., seismic monitoring, soil properties) are required to further refine the mapping.

3. Results

All six indicators were processed into normalized hazard layers. Slope analysis showed that ~34 % of the basin exceeds 25°, with the steepest values concentrated along reservoir-facing escarpments and major fault zones. Lithology strongly influenced susceptibility: weak Neogene–Quaternary deposits (22 % of the area) received the highest scores, while resistant granites and limestones correspond to the lowest values. NDWI composites for October (2000–2024) revealed persistent moisture along valley bottoms and steep slopes; 18 % of pixels exceeded 0.25, indicating shallow water or wet vegetation. Lineament density mapping emphasized structural corridors parallel to the Kumbel–Ugam and North Pskem faults, where clustering of linear features suggests enhanced crustal weakness. Distance indicators further highlighted zones within 500 m of faults and <1 km from the shoreline as particularly sensitive to instability.

The AHP weighting scheme emphasized slope gradient (0.28) and lineament density (0.24) as dominant factors, followed by lithology (0.18), NDWI (0.15), distance to faults (0.09), and distance to shoreline (0.06). These weights reflect the specific geomorphological setting of the Charvak basin, where steep terrain and structural discontinuities strongly control slope instability. Their integration produced a continuous composite hazard index (Fig. 4), with values clustering in structurally active and moisture-saturated zones.

The composite index was classified into five hazard categories (very low to very high) using Jenks natural breaks. High and very high hazard

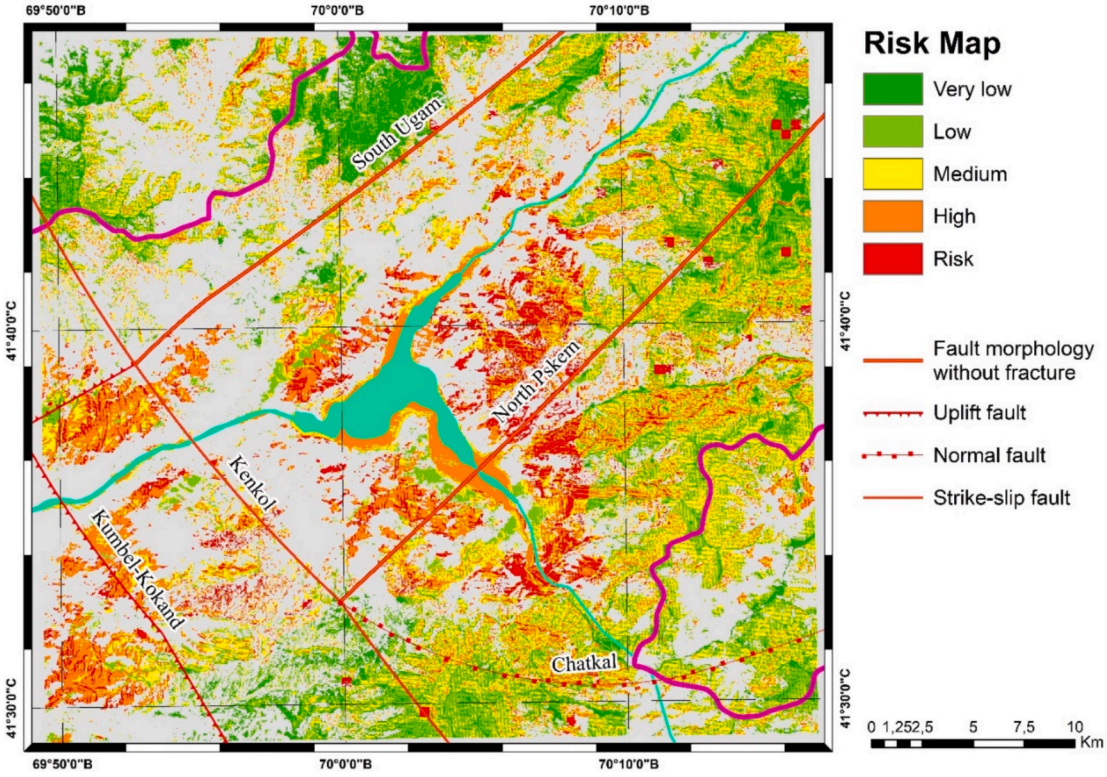

Fig. 4. Spatial distribution of risk classes in the Charvak region.

Table 4
Area distribution by geohazard class.

Hazard class	Area (km^2)	Proportion of Study Area (%)
Very low	18.6	9.3
Low	43.2	21.6
Medium	65.4	32.7
High	48.7	24.3
Very high (Risk)	22.1	11.1

zones occupy ~19 % of the basin, concentrated on steep reservoir-facing slopes, structurally controlled escarpments, and moist valley floors. Moderate hazard zones cover 33 %, while low and very low classes together account for 48 %, corresponding mainly to resistant lithologies and gentle terrain. The proportional extent of each class is summarized in Table 4, and the spatial distribution is shown in Fig. 4.

4. Discussion

4.1. Influence of conditioning factors

The weighting results confirm slope gradient and lineament density as the dominant conditioning factors for slope-related geohazards in the Charvak basin. Steep reservoir-facing slopes (>25°) are strongly associated with mass movement processes, consistent with findings from other mountainous reservoirs (Arabameri et al., 2018). High lineament density reflects zones of structural weakness and corresponds to fault-controlled escarpments, supporting previous studies in Central Asia that showed structural discontinuities play a major role in slope instability (Juliev et al., 2017). Lithology further differentiated weak Neogene–Quaternary sediments, which are prone to failure, from stable carbonate and intrusive rocks. NDWI composites highlighted persistent moisture zones along valley bottoms and steep slopes, which correlate with known landslide-prone areas. Distances to faults and the shoreline contributed less to the overall model but remain relevant for localized instability linked to seismic sensitivity and reservoir-induced processes (Gupta, 2022; Talwani, 1997).

4.2. Comparison with previous work

Our results are consistent with earlier geomorphological and tectonic studies in the western Tien Shan, which emphasized the role of steep slopes and active faulting in controlling slope-related hazards (Khamidov et al., 2021; Umurzakov, 2012). Similar to the findings of Juliev et al. (2019) and Petrov et al. (2017), the highest susceptibility classes in our model cluster along the eastern and southern margins of the Charvak Reservoir, where structural corridors intersect with steep reservoir-facing slopes. Independent mapping of landslides in these areas, including the historically active Mingchukur site, corroborates our identification of these slopes as particularly unstable. Compared with earlier single-factor analyses, our AHP-based model provides a more integrated framework. For example, Petrov et al. (2017) focused on deformation zones identified using InSAR and optical imagery, whereas our model combines six conditioning factors, including NDWI and lineament density, which indirectly capture moisture dynamics and structural discontinuities. This explains why our hazard zonation highlights not only the well-known southern slopes but also previously underreported moist valley floors, which accounted for ~18 % of NDWI pixels exceeding 0.25.

Our results also align with Khamidov et al. (2023), who demonstrated that reservoir-induced hydrological loading contributes to near-surface stress changes and microseismicity. The spatial coincidence between our high-susceptibility zones and clusters of shallow earthquakes (<10 km) along the North Pskem and Kumbel–Ugam faults supports their conclusions on reservoir–tectonic interactions. Furthermore, lithological contrasts highlighted in our model agree with the mechanical instability of Neogene–Quaternary units reported by Maksudov et al. (2021), which represent 22 % of the basin and consistently coincide with high hazard classes.

Beyond slope instability, upstream hazard processes such as glacial

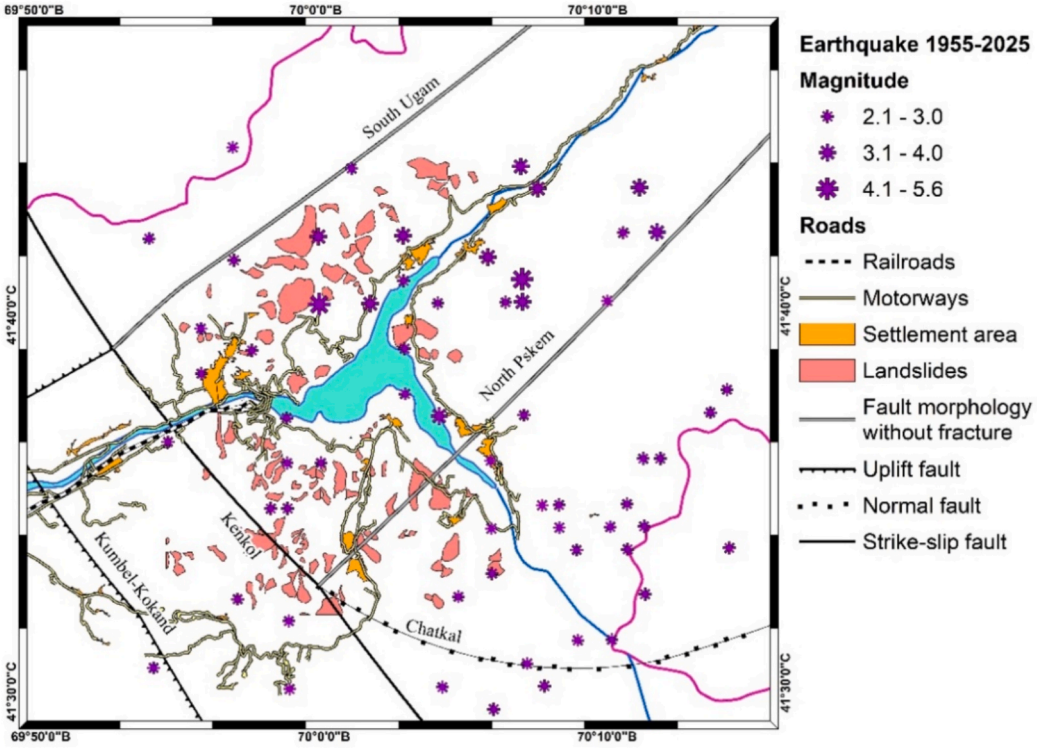

Fig. 5. Distribution of mapped landslides and seismic events (1955–2025) in the Charvak basin, shown in relation to major fault zones and settlements (Juliev et al., 2017; Tsay, 2019).

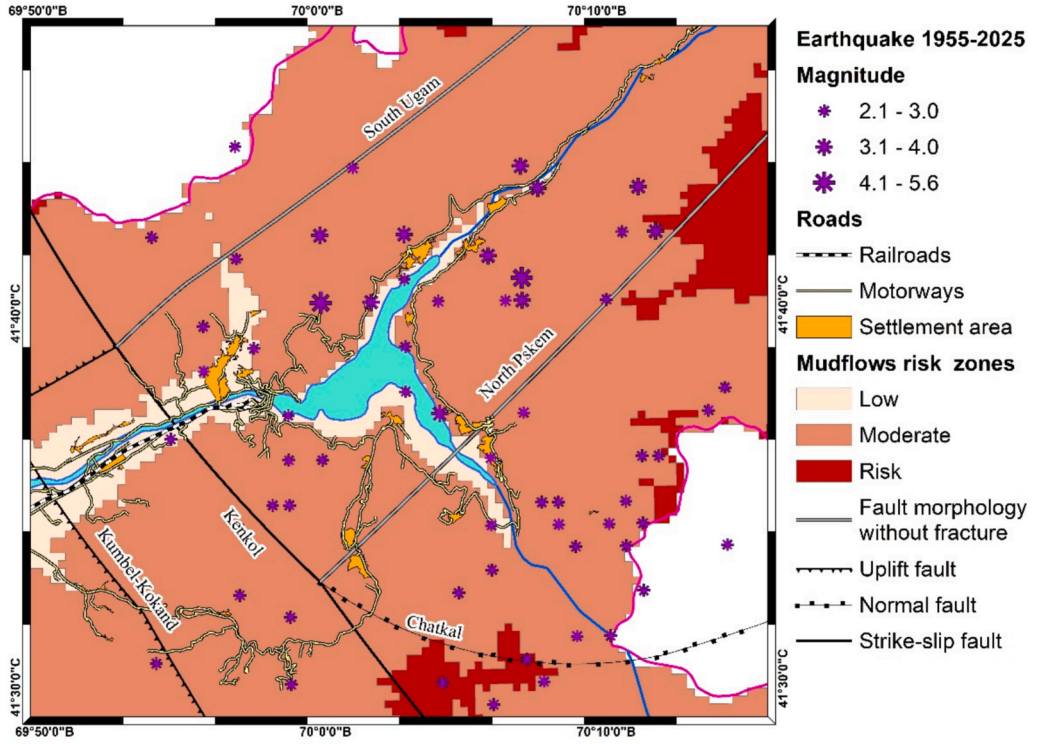

Fig. 6. Independently mapped mudflow hazard zones (Aksenova et al., 2008) in the Charvak basin.

lake outburst floods (Hoelzle et al., 2017; Wang et al., 2018) remain an important component of the regional risk environment. While these were not directly modeled here, their spatial proximity to the Pskem and Chatkal catchments reinforces the need for future multi-hazard assessments that combine slope, seismic, and cryospheric factors.

In addition to comparisons with the literature, the hazard map was validated against independent datasets of mapped landslides and mudflow-prone zones (Figs. 5 and 6). The distribution of known

landslides and seismic events from 1955 to 2025 (Fig. 5) shows a strong spatial coincidence with modeled high- and very high-susceptibility classes, with more than 70 % of documented events located within these zones. Similarly, previously delineated mudflow hazard areas (Fig. 6) exhibit substantial overlap, with approximately 68 % falling into the moderate to high susceptibility categories. This quantitative agreement demonstrates that the multi-criteria approach not only identifies theoretical hazard potential but also reliably captures observed instability patterns. The integration of these independent datasets thus reinforces the validity of the model and highlights its practical value for regional planning, infrastructure safety, and disaster risk reduction in the Charvak basin.

Overall, the strong agreement between our susceptibility map and published studies demonstrates both the reliability of the AHP–GIS approach and its added value compared with single-factor or qualitative assessments. By integrating multiple indicators within a transparent weighting scheme, our model advances previous efforts and provides a replicable methodology for hazard assessment in other mountainous and data-limited regions.

4.3. *Infrastructure and socio-economic exposure*

The hazard model was further evaluated by overlaying the susceptibility map (Fig. 4; Table 4) with infrastructure and settlement data (Figs. 5 and 6). The results indicate that 27 % of the regional road network and 21 % of villages and recreational facilities are located within high- and very high-susceptibility zones. Tourism infrastructure is particularly exposed along the eastern and southern reservoir margins, where roads and guesthouses are situated directly beneath unstable slopes. These quantitative overlaps demonstrate that the model effectively identifies areas of socio-economic vulnerability, underscoring its importance for risk-informed territorial planning and the sustainable development of the Charvak Free Tourist Recreation Zone.

4.4. *Methodological considerations and limitations*

The proposed model provides a relative susceptibility framework rather than a deterministic prediction of future failures. Although AHP weighting offers a transparent procedure, it remains partly subjective and assumes fixed relationships among conditioning factors. The resolution of input data also introduces uncertainties: Landsat-derived NDWI (30 m) cannot fully capture small-scale slope failures, and the SRTM DEM may smooth local relief. In addition, lineaments extracted from satellite imagery do not necessarily represent active tectonic faults, and field validation is required to distinguish structural features of geodynamic significance. Seasonal variations in moisture, seismic triggers, and anthropogenic influences were only indirectly represented in the current approach. Future work should therefore incorporate higher-resolution DEMs, GNSS-based deformation monitoring, and detailed geological field surveys to refine hazard zonation and enhance the transferability of the model to other mountainous basins.

5. Conclusion

This study developed a multi-criteria GIS model to assess slope-related geohazards in the Charvak Reservoir area, an ecologically sensitive and socioeconomically important mountain basin in Uzbekistan. By integrating six geospatial indicators—slope, lithology, lineament density, NDWI, and distances to active faults and the reservoir—the model delineated zones of high and very high susceptibility concentrated along steep reservoir-facing slopes, fault-controlled escarpments, and persistently moist terrain. The results are consistent with independent landslide and mudflow inventories as well as seismic records, confirming the robustness of the approach. Importantly, 21 % of villages and tourism facilities and 27 % of the regional road network are located within the highest hazard zones, underscoring the urgent need for risk-informed territorial planning in the Charvak Free Tourist Recreation Zone. Beyond its local application, the model demonstrates the broader value of integrating remote sensing, GIS, and AHP-based weighting for geohazard zonation in other data-limited mountain regions. Future research should incorporate higher-resolution datasets and field validation to refine hazard zonation and enhance model transferability. Nevertheless, the present study provides a replicable framework that can directly support regional planning, disaster risk reduction strategies, and the sustainable development of mountainous reservoir environments.

CRediT authorship contribution statement

Dilbarkhon Fazilova: Writing – review & editing, Writing – original draft, Validation, Project administration, Methodology, Funding acquisition, Data curation, Conceptualization. **Khasan Magdiev:** Visualization, Validation, Investigation, Data curation. **Mirshodjon Makhmudov:** Writing – original draft, Validation, Software, Investigation, Data curation. **Alisher Fazilov:** Software, Data curation.

Declaration of competing interest

The authors declare that they have no known competing financial interests or personal relationships that could have appeared to influence the work reported in this paper.

Acknowledgement

This research was conducted as part of project No. FL-8824063217, supported by the Agency of Innovative Development under the Ministry of Higher Education, Science, and Innovation of the Republic of Uzbekistan.

References

Abella, E.A.C., Van Westen, C.J., 2007. Generation of a landslide risk index map for Cuba using spatial multi-criteria evaluation. Landslides 4, 311–325. https://doi.org/10.1007/s10346-007-0087-y.

Aksenova, L., Aytbaev, D., et al., 2008. Atlas. Assessment of the Environmental State of Uzbekistan based on Environmental Indicators. Cartography, Tashkent.

Aleotti, P., Chowdhury, R., 1999. Landslide hazard assessment: summary review and new perspectives. Bull. Eng. Geol. Environ. 58, 21–44. https://doi.org/10.1007/s100640050066.

Alikhanov, B., Alikhanova, Sh., Oymatov, R., Fayzullaev, Z., Pulatov, A., 2020. Land cover change in Tashkent province during 1992–2018. IOP Conference Series: Materials Science and Engineering. 883, 012088. doi:10.1088/1757-899X/883/1/012088.

Al-Taani, A., Al-Husban, Y., Ayan, A., 2023. Assessment of potential flash flood hazards concerning land use/land cover in Aqaba Governorate, Jordan, using a multi-criteria technique. Egypt. J. Remote Sens. Space Sci. 26 (1), 17–24. https://doi.org/10.1016/j.ejrs.2022.12.007.

Arabameri, A., Rezaei, K., Pourghasemi, H.R., et al., 2018. GIS-based gully erosion susceptibility mapping: a comparison among three data-driven models and AHP knowledge-based technique. Environ. Earth Sci. 77, 628. https://doi.org/10.1007/s12665-018-7808-5.

Bachri, S., Shrestha, R., Sumarmi, S., Aksa, F.I., Regina, M., Putri, R., Billah, E., Hakiki, A. R., Hidiyah, T.M., 2024. Optimizing tourism development through landslide hazard mapping in Raung Volcano. Jurnal Geografi. 16, 1–16. https://doi.org/10.24114/jg.v16i1.50118.

Bathrellos, G.D., Skilodimou, H.D., Chousianitis, K., Youssef, A.M., Pradhan, B., 2017. Suitability estimation for urban development using multi-hazard assessment map. Sci. Total Environ. 575, 119–134. https://doi.org/10.1016/j.scitotenv.2016.10.025.

Bellendir, E.N., Aleksandrov, A.V., 2023. Mullalaq HPP on the River Pskem. Power Technol. Eng. 57 (6), 560–567. https://doi.org/10.1007/s10749-024-01698-x.

Bera, A., Mukhopadhyay, B.P., Das, D., 2019. Landslide hazard zonation mapping using multi-criteria analysis with the help of GIS techniques: a case study from Eastern Himalayas, Namchi, South Sikkim. Nat. Hazards 96, 935–959. https://doi.org/10.1007/s11069-019-03580-w.

Chen, T., Niu, R., Du, B., Wang, Y., 2015. Landslide spatial susceptibility mapping by using GIS and remote sensing techniques: a case study in Zigui County, the three Georges Reservoir, China. Environ. Earth Sci. 73, 5571–5583.

Cheng, J., Dai, X., Wang, Z., Li, J., Qu, G., Li, W., Wang, Y., 2022. Landslide susceptibility assessment model construction using typical machine learning for the three Gorges Reservoir Area in China. Remote Sens. (Basel) 14 (9), 2257. https://doi.org/10.3390/rs14092257.

Cui, H., Ji, J., Hürlimann, M., Medina, V., 2024. Probabilistic and physically-based modelling of rainfall-induced landslide susceptibility using integrated GIS-FORM

algorithm. Landslides 21 (6), 1461–1481. https://doi.org/10.1007/s10346-023-02094-0.
Dai, F.C., Lee, C.F., Ngai, Y.Y., 2002. Landslide risk assessment and management: an overview. Eng. Geol. 64 (1), 65–87. https://doi.org/10.1016/S0013-7952(01)00093-X.
Das, S., Sarkar, S., Kanungo, D., 2022. GIS-based landslide susceptibility zonation mapping using the analytic hierarchy process (AHP) method in parts of Kalimpong Region of Darjeeling Himalaya. Environ. Monit. Assess. 194 (3), 234. https://doi.org/10.1007/s10661-022-09851-7.
Dong, J.J., Tung, Y.H., Chen, C.C., Liao, J.J., Pan, Y.W., 2011. Logistic regression model for predicting the failure probability of a landslide dam. Eng. Geol. 117 (1–2), 52–61. https://doi.org/10.1016/j.enggeo.2010.10.003.
Drummer, T.D. 1998. Generalized Geology of the Former Soviet Union (geo1ec). U.S. Geological Survey data release. doi:10.5066/P9GUL0PQ.
Elkhrachy, I., 2015. Flash flood hazard mapping using satellite images and GIS tools: a case study of Najran City, Kingdom of Saudi Arabia (KSA). Egypt. J. Remote Sens. Space Sci. 18 (2), 261–278. https://doi.org/10.1016/j.ejrs.2015.06.007.
Fang, Z., Wang, Y., Duan, G., Peng, L., 2021. Landslide susceptibility mapping using rotation forest ensemble technique with different decision trees in the three Gorges Reservoir Area, China. Remote Sens. (Basel) 13 (2), 238. https://doi.org/10.3390/rs13020238.
Fazilova, D., Magdiev, K., Sichugova, L., 2021. Vertical accuracy assessment of open access digital elevation models using GPS. Int. J. Geoinform. 17 (1), 19–26. https://doi.org/10.52939/ijg.v17i1.1701.
Fazilova, D., Magdiev, Kh., Makhmudov, M., Kabilov, Kh., 2026. Lineament analysis and water level variations in the geodynamic assessment of the Charvak Reservoir Area, Uzbekistan (2022–2024). Int. J. Eng. Geosci. 11 (1), 89–105. https://doi.org/10.26833/ijeg.1652490.
Fazilova, D., Makhmudov, M., Khalimov, B., 2025. The analysis of crustal deformation patterns in the Tashkent region, Uzbekistan, derived from GNSS data over the period 2018–2023. Geod. Geodyn. 16 (2), 137–146. https://doi.org/10.1016/j.geog.2024.07.001.
Fentahun, T.M., Bagyaraj, M., Melesse, M.A., Korme, T., 2021. Seismic hazard sensitivity assessment in the Ethiopian Rift, using an integrated approach of AHP and DInSAR methods. Egypt. J. Remote Sens. Space Sci. 24 (3), 735–744. https://doi.org/10.1016/j.ejrs.2021.05.001.
Gao, B., 1996. NDWI—A normalized difference water index for remote sensing of vegetation liquid water from space. Remote Sens. Environ. 58 (3), 257–266. https://doi.org/10.1016/S0034-4257(96)00067-3.
Gill, J.C., Malamud, B.D., 2014. Reviewing and visualizing the interactions of natural hazards. Rev. Geophys. 52, 680–722. https://doi.org/10.1002/2013RG000445.
Gupta, H.K., 2022. Artificial water reservoir-triggered seismicity (RTS): Most prominent anthropogenic seismicity. Surv. Geophys. 43 (2), 619–659. https://doi.org/10.1007/s10712-021-09675-z.
Hoelzle, M., Usubaliev, R., Gafurov, A., Kronenberg, M., Wagnon, P., Petrakov, D., Kääb, A., 2017. Re-establishing glacier monitoring in Kyrgyzstan and Uzbekistan, Central Asia. Geosci. Instrum. Methods Data Syst. 6 (2), 397–418. https://doi.org/10.5194/gi-6-397-2017.
Hu, J., Chen, J., Chen, Z., Cao, J., Wang, Q., Zhao, L., Chen, G., 2018. Risk assessment of seismic hazards in hydraulic fracturing areas based on fuzzy comprehensive evaluation and AHP method (FAHP): a case analysis of Shangluo area in Yibin City, Sichuan Province, China. J. Petrol. Sci. Eng. 170, 797–812. https://doi.org/10.1016/j.petrol.2018.06.066.
Jena, R., Pradhan, B., 2020. Integrated ANN-cross-validation and AHP-TOPSIS model to improve earthquake risk assessment. Int. J. Disaster Risk Reduct. 50, 101723. https://doi.org/10.1016/j.ijdrr.2020.101723.
Jenks, G.F., 1967. The data model concept in statistical mapping. Int. Yearbook Cartogr. 7, 186–190.
Juliev, M., Pulatov, A., Hubl, J., 2017. Natural hazards in mountain regions of Uzbekistan: a review of mass movement processes in Tashkent province. Int. J. Sci. Eng. Res. 8 (2), 1101–1108.
Juliev, M., Pulatov, A., Fuchs, S., Hübl, J., 2019. Analysis of land use land cover change detection of Bostanlik District, Uzbekistan. Pol. J. Environ. Stud. 28 (5), 3235–3242. https://doi.org/10.15244/pjoes/94216.
Kadapa, H., 2024. A comprehensive framework for landslide risk assessment of archaeological sites in Gujarat, India. Egypt. J. Remote Sens. Space Sci. 27 (1), 41–51. https://doi.org/10.1016/j.ejrs.2024.01.002.
Karpouza, M., Bathrellos, G.D., Kaviris, G., Antonarakou, A., Skilodimou, H.D., 2023. How could students be safe during flood and tsunami events? Int. J. Disaster Risk Reduct. 95, 103830. https://doi.org/10.1016/j.ijdrr.2023.103830.
Khamidov, L., Turapov, M., Mahkamov, S., Artikov, F., Suyunov, S., 2021. Tracking the local seismicity level in the active influence zone of the southern Uzbekistan reservoirs. E3S Web Conf. 264, 02043. https://doi.org/10.1051/e3sconf/202126402043.
Khamidov, L., Artikov, F., Khamidov, K., Ganieva, B., Anvarova, S., 2023. Seismicity caused by hydrological regime of large reservoirs. E3S Web Conf. 386, 03043. https://doi.org/10.1051/e3sconf/202338603043.
Kumari, M., Somvanshi, S., Sharma, R., Zubair, S., 2022. Analysis of multi-temporal remotely sensed spectral indices influence on ecology of Singrauli sub-district, Madhya Pradesh using an ecological impact index. Egypt. J. Remote Sens. Space Sci. 25 (3), 863–871. https://doi.org/10.1016/j.ejrs.2022.08.005.
Leonardi, G., Palamara, R., Manti, F., Tufano, A., 2022. GIS-multicriteria analysis using AHP to evaluate the landslide risk in road lifelines. Appl. Sci. 12 (9), 4707. https://doi.org/10.3390/app12094707.
Lee, S., Evangelista, D.G., 2006. Earthquake-induced landslide-susceptibility mapping using an artificial neural network. Nat. Hazards Earth Syst. Sci. 6, 687–695. https://doi.org/10.5194/nhess-6-687-2006.
Makhmudov, M., Fazilova, D., 2023. Construction of the velocity field in a regular grid in the Tashkent region on the basis of interpolation of GNSS permanent stations data. InterCarto. InterGIS. GI Support of Sustainable Development of Territories: Proceedings of the International Conference. 29 (1), 535–545. doi:10.35595/2414-9179-2023-1-29-535-545.
Maksudov, S.K., Abdullabekov, K.N., Tuichiev, A.I., et al., 2021. Geomagnetic field variations caused by the processes occurring at different depths in the Earth's crust and upper mantle. Izv. Phys. Solid Earth 57, 295–308. https://doi.org/10.1134/S1069351321020063.
McFeeters, S.K., 1996. The use of the Normalized Difference Water Index (NDWI) in the delineation of open water features. Int. J. Remote Sens. 17 (7), 1425–1432.
Mokhtari, D., Moazzez, S., Mohammadzadeh Golani, F., 2017. An investigation of the effect of some hydro-geomorphological factors on water supply and allocation of settlements by applying the analysis of hierarchical process (AHP). Hydrogeomorphology 4 (10), 1–19.
Moore, G.K., 1983. Objective procedures for lineament enhancement and extraction. Photogramm. Eng. Remote Sens. 49 (5), 641–647.
Petrov, M.A., Sabitov, T.Y., Tomashevskaya, I.G., Glazirin, G.E., Chernomorets, S.S., Savernyuk, E.A., Tutubalina, O.V., Petrakov, D.A., Sokolov, L.S., Dokukin, M.D., Mountrakis, G., Ruiz-Villanueva, V., Stoffel, M., 2017. Glacial lake inventory and lake outburst potential in Uzbekistan. Sci. Total Environ. 592, 228–242. https://doi.org/10.1016/j.scitotenv.2017.03.068.
Pospíšil, L., Bartoněk, D., Bures, J., et al., 2025. Identification and verification of geodynamic risk zones in the Western Carpathians using remote sensing, geophysical and GNSS data. Surv. Geophys. 46, 227–257. https://doi.org/10.1007/s10712-024-09870-8.
Plotnikova, L.M., Makhmudova, V.I., Sigalova, O.B., 1992. Seismicity associated with the Charvak reservoir, Uzbekistan. Pure Appl. Geophys. 139, 607–608. https://doi.org/10.1007/BF00879953.
Ramachandra, T.V., Setturu, B., Rajan, K.S., Chandran, M.D.S., 2016. Stimulus of developmental projects to landscape dynamics in Uttara Kannada, Central Western Ghats. Egypt. J. Remote Sens. Space Sci. 19 (2), 175–193. https://doi.org/10.1016/j.ejrs.2016.09.001.
Rakhmatullaev, S., Huneau, F., Celle-Jeanton, H., et al., 2013. Water reservoirs, irrigation and sedimentation in Central Asia: a first-cut assessment for Uzbekistan. Environ. Earth Sci. 68, 985–998. https://doi.org/10.1007/s12665-012-1802-0.
Reichenbach, P., Rossi, M., Malamud, B.D., Mihir, M., Guzzetti, F., 2018. A review of statistically-based landslide susceptibility models. Earth Sci. Rev. 180, 60–91. https://doi.org/10.1016/j.earscirev.2018.03.001.
Romero-Andrade, R., Trejo-Soto, M.E., Nayak, K., Hernández-Andrade, D., Bojorquez-Pacheco, N., 2023. Lineament analysis as a seismic precursor: The El Mayor Cucapah earthquake of April 4, 2010 (MW7.2), Baja California, Mexico. Geodesy Geodyn. 14 (2), 121–129. https://doi.org/10.1016/j.geog.2022.08.001.
Roy, D.P., et al., 2010. Web-enabled Landsat Data (WELD): Landsat ETM+ composited mosaics of the conterminous United States. Remote Sens. Environ. 114 (1), 35–49. https://doi.org/10.1016/j.rse.2009.08.011.
Saaty, T.L., 1990. How to make a decision: the analytic hierarchy process. Eur. J. Oper. Res. 48 (1), 9–26. https://doi.org/10.1016/0377-2217(90)90057-I.
Sharipov, Sh., Shomurodova, Sh., Gudalov, M., 2020. The use of the mountain kars in the tourism sphere in cort and recreation zone of Chimgan-Charvak. J. Crit. Rev. 7 (3), 475–481. https://doi.org/10.31838/jcr.07.03.87.
Shevyrev, S., Carranza, E.J.M., 2020. Modelling of geodynamic regimes of precious metal-bearing porphyry deposits: Lazurnoe deposit (Sikhote–Alin Belt, Far East) case study. Geol. J. 55 (12), 8309–8328. https://doi.org/10.1002/gj.3935.
Sichugova, L.V., Fazilova, D.S., 2020. Structural interpretation of lineaments using satellite image processing: a case study in the vicinity of the Charvak reservoir. InterCarto. Intergis. GI Support of Sustainable Development of Territories: Proceedings of the International Conference. 26 (2), 436–442. https://doi.org/10.35595/2414-9179-2020-2-26-436-442.
Sichugova, L., Fazilova, D., 2021. The lineaments as one of the precursors of earthquakes: a case study of Tashkent geodynamical polygon in Uzbekistan. Geod. Geodyn. 12 (6), 399–404. https://doi.org/10.1016/j.geog.2021.08.002.
Skilodimou, H.D., Bathrellos, G.D., Chousianitis, K., Youssef, A.M., Pradhan, B., 2019. Multi-hazard assessment modeling via multi-criteria analysis and GIS: a case study. Environ. Earth Sci. 78 (2), 47. https://doi.org/10.1007/s12665-018-8003-4.
Talwani, P., 1997. On the nature of reservoir-induced seismicity. Pure Appl. Geophys. 150, 473–492. https://doi.org/10.1007/s000240050089.
Tsay, O., 2019. Electronic map of faults of the Middle, Southern Tien Shan and adjacent territories. Proceedings of the LI Tectonic Meeting "Fundamental Problems of Tectonics and Geodynamics". 2, 382–386. http://www.ginras.ru/materials/files/MTS-2020-2%20.pdf.
Umurzakov, M., 2012. Neotectonics and focal mechanisms of earthquakes in the Tien-Shan: evidence from field and morphotectonic data. C. R. Geosci. 344 (3–4), 239–246. https://doi.org/10.1016/j.crte.2012.03.003.
Umurzakov, R.A., Muminov, M.Y., 2017. Studying of kinematics and elements of tension of blocks of the massif according to field geological observations. World J Mech. 7, 243–254. https://doi.org/10.4236/wjm.2017.79020.
Verma, N., Patel, R.K., 2021. Delineation of groundwater potential zones in lower Rihand River Basin, India using geospatial techniques and AHP. Egypt. J. Remote Sens. Space Sci. 24 (3), 559–570. https://doi.org/10.1016/j.ejrs.2021.03.005.
Xu, H., 2006. Modification of normalised difference water index (NDWI) to enhance open water features in remotely sensed imagery. Int. J. Remote Sens. 27 (14), 3025–3033. https://doi.org/10.1080/01431160600589179.

Wang, W., Yao, Y., Gao, J., 2018. Evolution and hazard assessment of glacial lakes in the Tien Shan–Pamir region. Geoenviron. Disasters 5 (1), 1–13. https://doi.org/10.1186/s40677-018-0095-4.

White, J.C., et al., 2014. Pixel-based image compositing for large-area dense time series applications and science. Can. J. Remote. Sens. 40, 192–212. https://doi.org/10.1080/07038992.2014.945827.

Wu, C., Zhang, P., Zhang, Z., Zheng, W., Xu, B., Wang, W., et al., 2023. Slip partitioning and crustal deformation patterns in the Tianshan orogenic belt derived from GPS measurements and their tectonic implications. Earth Sci. Rev. 238, 104362. https://doi.org/10.1016/j.earscirev.2023.104362.

Ye, Q., Wang, Y., Liu, L., Guo, L., Zhang, X., Dai, L., Zhai, L., Hu, Y., Ali, N., Ji, X., Ran, Y., Qiu, Y., Shi, L., Che, T., Wang, N., Li, X., Zhu, L., 2024. Remote sensing and modeling of the cryosphere in High Mountain Asia: a multidisciplinary review. Remote Sens. (Basel) 16 (10), 1709. https://doi.org/10.3390/rs16101709.

Zandi, R., Pari Far, G.S., 2025. Evaluating the factors affecting landslides using machine learning algorithms (case study: the catchment area of Karun-3 Dam, Iran). Egypt. J. Remote Sens. Space Sci. 28 (3), 512–522. https://doi.org/10.1016/j.ejrs.2025.07.005.

Zzaman, R.U., Nowreen, S., Billah, M., Islam, A.S., 2021. Flood hazard mapping of Sangu River basin in Bangladesh using multi-criteria analysis of hydro-geomorphological factors. J. Flood Risk Manage. 14 (3), e12715. https://doi.org/10.1111/jfr3.12715.